BEN- GURION UNIVERSITY OF THE NEGEV

THE FACULTY OF ENGINEERING SCIENCES

DEPARTMENT OF ELECTRICAL & COMPUTER ENGINEERING

ACCELERATED MAGNETIC RESONANCE IMAGING BY ADVERSARIAL NEURAL NETWORK

THESIS SUBMITTED IN PARTIAL FULFILLMENT OF THE REQUIREMENTS FOR THE MASTER OF SCIENCES DEGREE

OHAD SHITRIT

UNDER THE SUPERVISION OF: DR TAMMY RIKLIN-RAVIV

Feb 28, 2018

BEN- GURION UNIVERSITY OF THE NEGEV

THE FACULTY OF ENGINEERING SCIENCES

DEPARTMENT OF ELECTRICAL & COMPUTER ENGINEERING

ACCELERATED MAGNETIC RESONANCE IMAGING BY ADVERSARIAL NEURAL NETWORK

THESIS SUBMITTED IN PARTIAL FULFILLMENT OF THE REQUIREMENTS FOR THE MASTER OF SCIENCES DEGREE

OHAD SHITRIT

UNDER THE SUPERVISION OF: DR TAMMY RIKLIN-RAVIV

Signature of student: _____ Date: 28/02/2018

Signature of supervisor: _____ Date: _____

Signature of chairperson

Of the committee for graduate studies: _____ Date: _____

Feb 28, 2018

Abstract

A main challenge in Magnetic Resonance Imaging (MRI) for clinical applications is speeding up scan time. Beyond the improvement of patient experience and the reduction of operational costs, faster scans are essential for time-sensitive imaging, where target movement is unavoidable, yet must be significantly lessened, e.g., fetal MRI, cardiac cine, and lungs imaging. Moreover, short scan time can enhance temporal resolution in dynamic scans, such as functional MRI or dynamic contrast enhanced MRI. Current imaging methods facilitate MRI acquisition at the price of lower spatial resolution and costly hardware solutions.

We introduce a practical, software-only framework, based on deep learning, for accelerating MRI acquisition, while maintaining anatomically meaningful imaging. This is accomplished by partial MRI sampling, while using an adversarial neural network to directly estimate the missing k-space samples. The inter-play between the generator and the discriminator networks enables the introduction of an adversarial cost in addition to a fidelity loss used for optimizing the peak signal-to-noise ratio (PSNR). Promising image reconstruction results are obtained for 3T and 1.5T brain MRI, from large publicly available dataset, where only 40%, 25% and 16.6% of the raw samples of each scan are used. To assess the clinical usability of the reconstructed images we also performed tissue segmentation and compared the results to those obtained by using the original fully-sampled images. Segmentation compatibility, measured in terms of Dice scores and Hausdorff distances, demonstrate the quality of the proposed MRI reconstruction with respect to other methods, including the widely-used Compressed Sensing.

Contents

1 Acknowledgments **5**

2 Introduction **6**
2.1 Magnetic Resonance Imaging (MRI) 6
2.2 MRI Acceleration 7
2.2.1 Classic methods 7
2.2.2 Data Driven Methods 8

3 Method **10**
3.1 K-space 10
3.2 Objective 10
3.3 Network Architecture 11

4 Experimental Results **13**
4.1 Random Gaussian Sampling 13
4.1.1 PSNR and SSIM 14
4.1.2 Brain Extraction - Skull Stripping 16
4.1.3 Brain Segmentation 17
4.2 Phase Encoding Sampling 20

5 Summary and Discussion **23**
5.1 Discussion 23
5.1.1 Acknowledgment 23

List of Tables

4.1 Error in PSNR, without masking 14
4.2 Error in PSNR, with masking 15
4.3 SSIM for different sampling factors 15
4.4 MHD - brain extraction 16
4.5 Segmentation Dice score for different sampling ratios 17
4.6 Error in PSNR 21

List of Figures

3.1 Under-sampling artifacts: the arrows illustrate the sampling methodology . 10
3.2 Framework architecture: G and D are the generator and discriminator networks, respectively. 12
3.3 Networks architecture. Both generator and discriminator input is a two-channel signal, real and imaginary. The number above each layer represents the output channels and all convolutional kernels are 3×3. 12

4.1 $2D$ Gaussian sampling masks 14
4.2 PSNR without masking error-bar 15
4.3 Example of brain extraction 16
4.4 Examples of reconstructed MR images from under-sampled k-space - Factor 6. 18
4.5 Examples of reconstructed MR images from under-sampled k-space - Factor 4. 19
4.6 Examples of reconstructed MR images from under-sampled k-space - Factor 2.5. 20
4.7 Examples of reconstructed MR images from under-sampled k-space. 22

.

Publications

1 Ohad Shitrit, Tzachi Hershkovich ,Tamar Shalmon, Ilan Shelef, and Tammy Riklin Raviv. Probabilistic model for 3D interactive segmentation, In MICCAI workshop on Interactive Medical Image Computing (IMIC), 2014.

2 Tzachi Hershkovich ,Ohad Shitrit, Tammy Riklin Raviv et al., T.R., 2016. Probabilistic model for 3D interactive segmentation. Computer Vision and Image Understanding, 151, pp.47-60. Vancouver

3 Ohad Shitrit and Tammy Riklin Raviv. Accelerated Magnetic Resonance Imaging by Adversarial Neural Network. In Deep Learning in Medical Image Analysis and Multimodal Learning for Clinical Decision Support (pp. 30-38). Springer, Cham.

4 TODO: add the Journal submission

Chapter 1

Acknowledgments

This was a great journey, challenging and educational. Thanks to all the amazing people that support, encouraged and guided me through these years.

First of all, I would like to thank to my supervisor, Dr. Tammy Riklin-Raviv, for guiding me in the last four years. Starting from the my undergraduate final project, during my master and my thesis research. Thanks for letting me be a part of one of the most fascinating filed of research. I admire your professionalism, dedication and your curiosity, which always been an inspiration for me. Tammy, thank you for the long hours of conversations, tips and guidances at any time, explaining theory and ideas in a simple and easy way to understand. All these are made me a better researcher and engineer.

Second, I want to thank to my lab colleagues, for a fruitful brainstormings, technical support and most important, being my friends. Great thanks to Tzachi Hershkovich, that was my partner of my undergraduate final project, I have learned a lot from you.

Last but not least, I want to thank to my life partner, my beloved wife Lee, for all your support during this journey. You encouraged me to be who I am today.

Chapter 2

Introduction

2.1 Magnetic Resonance Imaging (MRI)

Magnetic Resonance Imaging (MRI) is a non-ionizing imaging modality, and is therefore widely used in diagnostic medicine and biomedical research.

From MRI theory, we know that raw data collected from MR machines, the k-space values, which are RF signals at a predefined range of frequencies and phases.

Let's define G_{FE}, G_{PE} as the frequency and phase encoding gradients respectively. K-space is in a spatial frequency domain. The complex array of raw data points is treated as a two-dimensional grid of points (k_x, k_y) where k_x, k_y are defined as follows:

$$\begin{cases} k_x = \gamma G_{FE} t \\ k_y = \gamma G_{PE} T_{PE} \end{cases} \tag{2.1}$$

T_{PE} denotes the total time in which the respective gradient is active and $r\gamma$ is the gyromagnetic constant. The desired signal, a 2D MR image, is defined as the inverse Fourier transform of the encoded measured signal s_0, where $\Omega \subset \mathbb{R}^2$:

$$I(x, y) = \iint_{\Omega} s_0(k_x, k_y) e^{+j2\pi(k_x x + k_y y)} dk_x dk_y \tag{2.2}$$

As known from signal processing theory, lack of information in k-space will cause artifacts such as aliasing, blurring, and results in low resolution MR images. In some cases, decreasing the acquisition time is necessary for detecting temporal changes which can indicate certain illnesses.

2.2 MRI Acceleration

2.2.1 Classic methods

Magnetic Resonance Imaging (MRI) is a non-ionizing imaging modality, and is therefore widely used in diagnostic medicine and biomedical research. The physical principles of MRI are based on a strong magnetic field and pulses of radio frequency (RF) electromagnetic radiation. Images are produced when hydrogen atoms, which are prevalent in living organisms, emit the absorbed RF energy that is then received by antennas in close proximity to the anatomy being examined. Spatial localization of the detected MRI signals is obtained by varying the magnetic field gradients. The discretized RF output is presented in a Fourier space (called K-space), where the x-axis is refers to the frequency and the y-axis to the phase. An inverse fast Fourier transform (IFFT) of the K-space is then used for generating anatomically meaningful MRI scans. Figure 3.1 presents K-space traversal patterns used in conventional imaging. Each row of the k-space is acquired after one RF excitation pulse. The number of rows multiplied by the number of slices (z-axis) determines the total scan time.

The duration of standard single structural MRI acquisition is approximately 5 minutes. Usually, several scans of different modalities or a sequence of scans are acquired such that the overall scan time is much longer. Lengthy imaging process reduces patient comfort and is more vulnerable to motion artifacts. In cases where motion is inevitable, e.g., fetal MRI, cardiac cine, and lungs imaging, scan time must be significantly shortened, otherwise the produced images might be useless. Moreover, in dynamic MRI sequences, acquisition must be brief such that the temporal resolution of the sequence would allow capturing significant temporal changes, e.g., instantaneous increment of the contrast-enhanced material concentration in DCE-MRI or differences in hemodynamic response expressed in fMRI [?].

A straight forward reduction of the scan time can be obtained by sampling fewer slices, thus reducing the spatial resolution in the z-axis. Spatial distances between adjacent slices of fetal MRI or fMRI, for example, are often as high as 0.5 centimeters. Therefore, a significant portion of the potential input is not conveyed through imaging. On the other hand, under-sampling in the x-y domain leads to aliasing, as predicted by the Nyquist sampling theorem.

Numerous research groups as well as leading MRI scanner manufacturers make significant efforts to accelerate the MRI acquisition process. Hardware solutions allow parallel imaging by using multiple coils [?] to sample k-space data. There exist two major approaches [?] that are currently implemented in commercial MRI machines. Both reconstruct an image from the under-sampled k-space data provided by each of the coils. The sensitivity encoder (SENSE) transforms the partial k-spaces into images, then merges the resulting aliased images into one coherent image [?]. The GeneRalized Autocalibrating Partial Parallel Acquisition (GRAPPA) techniques [?] operate on signal data within the complex frequency domain before the IFFT.

The compressed sensing (CS) technique [?] allows efficient acquisition and re-

construction of a signal with fewer samples than the Nyquist-Shannon sampling theorem requires, if the signal has sparse representation in a known transform domain. Using CS for MRI reconstruction by sampling a small subset of the k-space grid had been proposed in [?]. The underlying assumption is that the undersampling is random, such that the zero-filled Fourier reconstruction exhibits incoherent artifacts that behave similarly to additive random noise. The smooth reconstruction obtained by the CS, may result in a loss of noise-like texture that can be anatomically meaningful.

2.2.2 Data Driven Methods

Recently different data driven, machine learning techniques were used for MRI acceleration. Ravishankar and Bresler [?] proposed a patch dictionary learning based method, for exploit the correlation between image patches in a static image in order to reconstruct MRI from highly under-sampled k-space data. In [?], an iterative algorithm for dictionary learning used for reconstruction of cardiac cine data with Cartesian k-space under sampling.

Manifold learning has been applied to reconstruction of dynamic MRI in many works. In [?], an hierarchical manifold learned from MR image patches, while each path manifold was consistent with the manifold trained on the entire image. In [?, ?], a compressive manifold structure, based on Laplacian eigenmaps, is reconstructed directly from the k-space. The first aims to estimate respiratory motion while the second make use of kernel regression for estimate cardiac motion.

A deep learning based methods open the gate to learn the reconstruction from a fully-sampled MR images. MRI reconstruction using convolutional neural networks (CNN) which learns the mapping between zero-filled and fully-sampled MR images was introduced in [?]. In [?], residual CNN was proposed for MRI super-resolution. Their model is able to receive multiple inputs acquired from different viewing planes for better image reconstruction.

Both [?, ?] suggests a multi-scale residual network, also known as U-net [?] for reconstruction of MR images. In [?], the CS problem was formulate as a residual regression problem and solved by a deep convolutional neural network that learned the aliasing artifacts. In [?], the U-net MR output image, is used for estimate the missing k-space samples. The fully k-space is then recovered by integrating the sampled k-space according to the sampling mask. Also for dynamic MRI reconstruction, a deep CNN has been successfully applied in [?] and provides better results over the time-consuming CS method. All these works address the reconstruction problem in the image domain rather than the k-space domain.

The proposed framework utilizes recent advances in deep learning, while similarly to the CS methods addresses MRI reconstruction directly from the k-space. Specifically, we use generative adversarial networks (GAN) [?, ?, ?]. GANs are based on the inter-play between two networks: a generator and a discriminator. The generator is capable of learning the distribution over a database, and sample realizations of this distribution. The discriminator is trained

to distinguish between 'generated' samples and real ones. This powerful combination has been used for MRI acceleration in [?, ?], and also for generating Computed Tomography (CT)-like images from MRIs [?]. Here, the generator is used for reconstruction of the entire k-space grid from under-sampled data. Its loss is a combination of an adversarial loss, based on the discriminator output and a fidelity loss with respect to the fully sampled MRI.

We compare the proposed method to reconstruction results obtained by using a conventional compressed sensing method CS-MRI [?] and Zero-filling. In addition, we optimize two networks: 1. CNN-L2 - a k-space generator (with same architecture as the proposed method) trained with only L2 loss. 2. IM-CNN-L2 - a network which performs on the image-space and optimized to remove the artifacts caused by under-sampling and zero padding. To assess the clinical usability of the reconstructed images we perform an extended validation, composed of anatomy and quantitative measurements. In addition to the common used PSNR and Structure Similarity Index (SSIM) we perform tissue segmentation and compared the results to those obtained by using the original fully-sampled images. Segmentation compatibility, measured in terms of Dice scores and Hausdorff distances, demonstrate the quality of the proposed MRI reconstruction with respect to other methods. The proposed method outperforms the other in 3T and 1.5T brain MRI reconstruction, using a large publicly available dataset, where only 40%, 25% and 16.6% of the raw samples of each scan are used. Moreover, compared to the widely used CS-MRI, the proposed method is faster in a two orders of magnitude. This makes it possible to use it in a real time manner.

Chapter 3

Method

3.1 K-space

Let $\boldsymbol{u}$ denote the desired signal, a 2D MR image, obtained by the IFFT of the complex k-space signal s_0. Let M_F denote a full sampling mask such that the reconstructed MR image is:

$$\boldsymbol{u} = F^H M_F \odot s_0 \tag{3.1}$$

where H is the Hermitian transpose operation, $\odot$ denotes element-wise multiplication, and F^H is an orthonormal 2D IFFT operator, such that $F^H F = I$. While sampling part of the k-space, using M_p as a sampling mask, the reconstructed MR image suffers from artifacts and aliasing. An example artifacts caused by under-sampling in the phase axis using Gaussian mask (40%) is shown in Figure **3.1**.

(a) raw k-space (b) fully sampled MRI (c) sampling mask (d) Zero-filled

Figure 3.1: Under-sampling artifacts: the arrows illustrate the sampling methodology

3.2 Objective

Let $s_p = M_p \odot s_0$ denote the under-sampled k-space. Given a sampling mask and a model f, defined by the set of parameters Θ, our goal is to estimate the

missing k-space samples such that:

$$\Theta = \arg\min_{\Theta} L(F^H f\left(s_p;\Theta\right), \boldsymbol{u}) \tag{3.2}$$

where $L\left(\cdot\right)$ is the loss function. While choosing the loss to be L2 norm is reasonable for natural images, for the k-space, which has different spatial features, this may not be enough. As mentioned in [?], L2 minimization provides a blurry solution, results in a loss of fine details. Averaging the high frequency details in the k-space domain results in very poor reconstruction. In order to address this problem, we used the adversarial loss, based on GAN.

We trained our model using the adversarial strategy, as described in [?, ?]. This method is based on a generator G, which takes noise z with uniform distribution $p_u\left(z\right)$ as input and generates samples from the data distribution. A discriminator D is trained to distinguish between "real" examples from the data and generated ("fake") examples from G. During the training process, we optimize G to maximize the discriminator's probability of error. Simultaneously, D is getting better and provides more accurate predictions.

Let s_0 denote a "real" k-space sample from the distribution $p_r\left(s_0\right)$. The following optimization process can be described by two-players min-max game:

$$\min_{G}\max_{D} \mathbb{E}_{\mathrm{s_0\sim p_r(s_0)}}\log\left[\mathrm{D\left(x\right)}\right] + \mathbb{E}_{\mathrm{z\sim p_u(z)}}\log\left[1-\mathrm{D\left(G(z)\right)}\right] \tag{3.3}$$

In equilibrium, the generator G is able to generate samples that look like the real data. In our case, G estimates the missing k-space samples from a linear combination of the sampled data and a uniform noise with distribution $p_u\left(z\right)$. An L2 fidelity constraint is added to the adverbial loss of the generator, as follows:

$$\begin{aligned} L_G = \alpha \cdot E_{\mathrm{z\sim p_u(z)}}\log\left[1-\mathrm{D}\left(\mathrm{F}^{-1}\left(\hat{\mathrm{s}}_0\right)\right)\right] + \\ \beta \cdot ||\left(1-M_p\right)\odot\left(\hat{s}_0 - s_0\right)||_2^2 \end{aligned} \tag{3.4}$$

where $\hat{s}_0$ is the estimated k-space and $\alpha = 1$, $\beta = 1$ are hyperparameters tuned by a cross-validation process. The discriminator's input is the reconstructed MR image, i.e., after IFFT. By that, we are integrating the reconstruction phase in our optimization. In this work, we use the Wasserstein distance as the GAN loss function [?] which helps us to improve the training stability and provides better reconstruction than the classic GAN.

3.3 Network Architecture

The generator input is a two-channel image representing the real and the imaginary parts of the partially sampled k-space image, s_p. Each missing sample is initialized by uniform i.i.d. noise. The pixel (i,j) in the generator input image is:

$$G_{in}\left(i,j\right) = s_{p_{i,j}} + \left(1-M_p\right)_{i,j} z_{i,j} \tag{3.5}$$

Due to the combination of the adversarial and the fidelity loss, G produces reasonable k-space samples from a given samples and noise distribution $p_u(z)$. In order to use the sampled data, s_p, and estimate only the missing samples we used a residual network [?] as used in [?], such that:

$$\hat{s}_0 = s_p + (1 - M_p) \odot G_{out} \tag{3.6}$$

where G_{out} is the generator output. Figure 3.2 describes our framework:

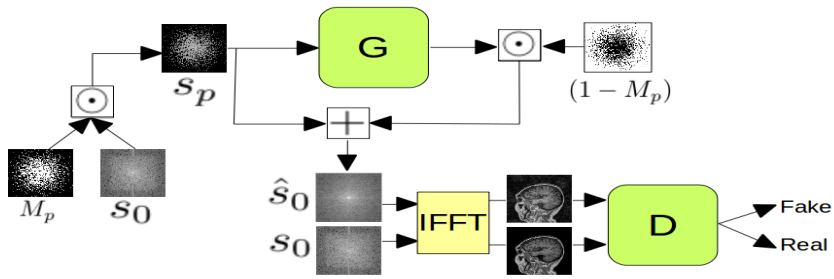

Figure 3.2: Framework architecture: G and D are the generator and discriminator networks, respectively.

A common architecture is used for the discriminator, composed of convolutional layers, batch normalization, and leaky-ReLU as suggested in [?]. For the generator, we compose a dedicated architecture based on multi-channel input for representing the real and imaginary components. Both architectures are shown in Figure 3.3. The training methodology is doing k_d discriminator update steps for each generator single step.

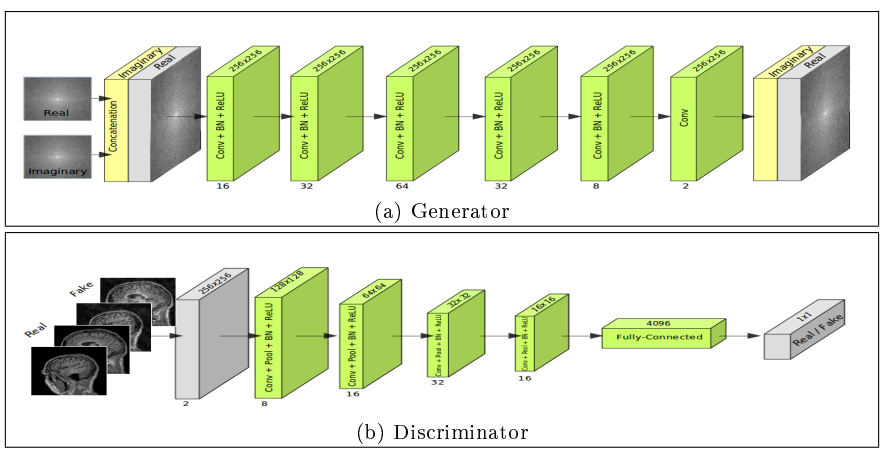

(a) Generator

(b) Discriminator

Figure 3.3: Networks architecture. Both generator and discriminator input is a two-channel signal, real and imaginary. The number above each layer represents the output channels and all convolutional kernels are 3×3.

Chapter 4

Experimental Results

4.1 Random Gaussian Sampling

The training data consists of 500 $3D$ brain MRI (T1) scans of different patients from the IXI dataset[1]. The data has been acquired by three MR machines, Philips 1.5T, 3T and GE 1.5T. All images padded to resolution of 256×256 pixels. From each $3D$ volume we extract 93 $2D$ saggital slices. We used $37.2k$ (80%) 2D slices for training and $9.2k$ (20%) for testing (100 $3D$ volumes). In order to create k-space images for training, inverse orthonormal 2D FFT is applied to the fully-sampled MR images. Further to our work [?], which was focused on Cartesian 2D sampling mask along the phase axis, we sample the k-space using $2D$ Gaussian mask, and achieve higher sampling factors of 2.5, 4 and 6 (Figure 4.1). Data augmentation is created by random offsets of the proposed mask and image flipping. This leads us to reconstruction of the MR image from 40%, 25% and 16.6% of the original k-space data.

The generator is composed of 5 blocks of CONV-BatchNorm-ReLU, with output channels $16, 32, 64, 32, 8$, respectively. The last layer is CONV with two outputs channels (for real and imaginary parts). The discriminator is composed of 4 blocks of CONV-Pool-BatchNorm-LReLU with output channels $8, 16, 32, 16$ and one fully-connected layer. All CONV layers kernel size is 3×3. All weights was initialized by Xavier [?]. We used RMSprop solver with fixed learning rate of 5e$-$6 and set k_d to 1.

We compare the proposed method to reconstruction results obtained by using a conventional compressed sensing method CS-MRI [?] and Zero-filling. In addition, we optimized two networks: 1. CNN-L2 - a k-space generator (with same architecture as the proposed method) trained with only L2 loss. 2. IM-CNN-L2 - a network which performs on the image-space and optimized to remove the artifacts caused by under-sampling and zero padding. We used the U-net [?] architecture and the same reconstruction method as presented in [?]. Specifically, we apply an FFT on the U-net output image to get an estimated k-space. The

[1] `http://brain-development.org/ixi-dataset/`

fully k-space is then recovered by integrating the sampled k-space according to the sampling mask. The same sampling masks was used for all methods.

To assess the clinical usability of the reconstructed images we perform an extended validation, composed of anatomy and quantitative measurements. In addition to the common used PSNR and Structure Similarity Index (SSIM) [?] metrics, we perform tissue segmentation and compared the results to those obtained by using the original fully-sampled images. The segmentation compatibility is measured in terms of Dice scores and Hausdorff distances.

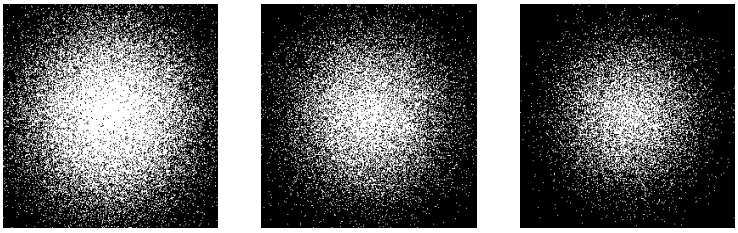

(a) Factor 2.5 (40%) (b) Factor 4 (25%) (c) Factor 6 (16.66%)

Figure 4.1: $2D$ Gaussian sampling masks

4.1.1 PSNR and SSIM

PSNR and SSIM are the most commonly used measures for evaluate image reconstruction quality. PSNR measures the Mean Squared Error (MSE) between the fully-sampled MR image and the reconstructed image. Therefore, this measure is not a sufficient metric for edges and general objects shape. For example, a model can provides a good reconstruction in the sense of PSNR but with blurry edges and loss of anatomical fine details. This leads to a poor segmentation, which used for medical diagnostic. However, PSNR is still a good indication for the image quality, especially if an expert should view it. Quantitative evaluation is presented in Table 4.1 and a graphical visualization in Figure 4.1.1. The PSNR calculated on the whole image without masking. Note that the proposed method outperforms the other.

PSNR Method	Factor 2.5	Factor 4	Factor 6
Zero-filled	32.555 ± 2.294	26.791 ± 1.856	16.781 ± 1.737
CS-MRI	39.053 ± 1.750	33.088 ± 1.929	26.491 ± 2.587
IM-CNN-L2	39.663 ± 1.934	35.042 ± 2.042	28.134 ± 2.181
CNN-L2	39.394 ± 1.985	33.829 ± 2.034	31.403 ± 2.040
Proposed	**40.211 ± 1.902**	**35.133 ± 1.870**	**32.040 ± 2.110**

Table 4.1: Error in PSNR, without masking

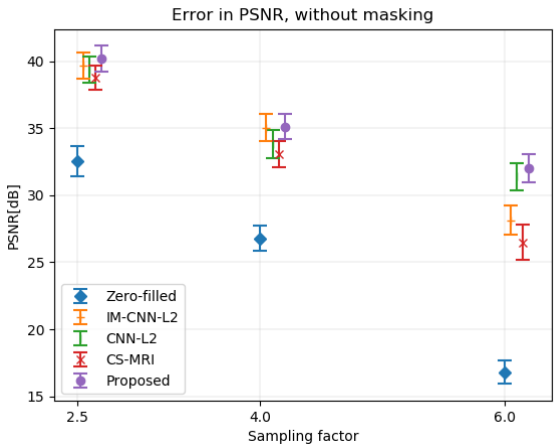

Figure 4.2: PSNR without masking error-bar

An additional validation of our model done by calculating the PSNR measure on different brain tissues. We applied an image segmentation algorithm, FAST [?], on the original fully-sampled MR image and then use it for calculating the masked-PSNR on gray matters, white matters and the Cerebrospinal Fluid (CSF). Results are presented in Table 4.2.

PSNR	Factor 2.5			Factor 4			Factor 6		
Method	White	Gray	CSF	White	Gray	CSF	White	Gray	CSF
Zero-filled	41.49±3.48	36.73±3.32	38.54±2.45	37.27±2.18	34.37±2.52	36.36±1.87	24.88±1.62	24.98±1.91	29.33±2.08
CS-MRI	44.37±4.20	40.04±3.84	40.74±3.16	41.65±3.12	37.24±2.99	39.11±2.43	35.59±3.15	33.11±2.91	36.64±2.26
IM-CNN-L2	45.66±4.60	41.06±4.27	41.51±3.58	43.47±3.22	39.36±3.19	40.16±2.51	37.34±3.19	34.18±2.85	36.61±2.10
CNN-L2	45.72±4.70	41.59±4.16	41.68±3.69	43.26±2.95	40.15±3.15	40.24±2.47	41.11±2.48	39.27±2.65	39.10±1.93
Proposed	**46.20±4.77**	**41.94±4.34**	**41.61±2.45**	**43.85±3.16**	**40.11±3.25**	**40.49±2.57**	**41.91±2.77**	**39.01±2.88**	**39.36±2.17**

Table 4.2: Error in PSNR, with masking

SSIM is used for measuring the similarity between the original and the reconstructed images. It quantifies the degradation caused by sampling artifacts based on visible structures in the image. SSIM values for different sampling factors are presented in Table 4.3.

SSIM Method	Factor 2.5	Factor 4	Factor 6
Zero-filled	0.698 ± 0.0452	0.590 ± 0.040	0.255 ± 0.021
CS-MRI	0.865 ± 0.029	0.757 ± 0.037	0.617 ± 0.030
IM-CNN-L2	0.884 ± 0.030	0.796 ± 0.036	0.606 ± 0.023
CNN-L2	0.885 ± 0.030	0.749 ± 0.043	0.682 ± 0.042
Proposed	**0.917 ± 0.019**	**0.818 ± 0.034**	**0.726 ± 0.038**

Table 4.3: SSIM for different sampling factors

4.1.2 Brain Extraction - Skull Stripping

Brain extraction (Skull stripping) is a an algorithm that delineates the brain boundary (Figure 4.3). It is necessary for almost every brain analysis algorithm. In tissue segmentation for example, skull stripping is a pre-processing step which affects directly on the segments partition. We examine the different reconstruction methods by applying the Brain Extraction Tool (BET) [**?**] on each different MR reconstructed image. Then, we compared the skull stripping results to the fully-sampled result using the Modified Hausdorff Distance (MHD) [**?**].

Let $C_1, C_2 \in R^2$ denotes the brain contours extract from skull stripping algorithm on two different reconstruction methods respectively (in our case the fully-sampled and the tested reconstruction method). MHD measures the distance between the contours such that:

$$\begin{gathered} MHD(C_1, C_2) = \max\left\{\frac{1}{|C_1|}\sum_{\sigma_1 \in C_1} d(\sigma_1, C_2),\ \frac{1}{|C_2|}\sum_{\sigma_2 \in C_2} d(\sigma_2, C_1)\right\} \\ d(\sigma_1, C_2) = \min_{\sigma_2 \in C_2} ||\sigma_1 - \sigma_2|| \\ d(\sigma_2, C_1) = \min_{\sigma_1 \in C_1} ||\sigma_2 - \sigma_1|| \end{gathered} \tag{4.1}$$

where σ_1, σ_2 are points on the contours C_1, C_2 respectively (Figure 4.3.c). MHD values for different sampling ratios are presented in Table 4.4.

MHD Method	Factor 2.5	Factor 4	Factor 6
Zero-filled	1.111 ± 0.563	2.617 ± 1.214	3.121 ± 1.279
CS-MRI	0.701 ± 0.511	1.447 ± 1.027	3.114 ± 1.617
IM-CNN-L2	0.541 ± 0.388	0.724 ± 0.394	1.902 ± 1.437
CNN-L2	0.420 ± 0.270	0.715 ± 0.561	1.083 ± 1.052
Proposed	**0.391 ± 0.250**	**0.617 ± 0.306**	**1.050 ± 1.033**

Table 4.4: MHD - brain extraction

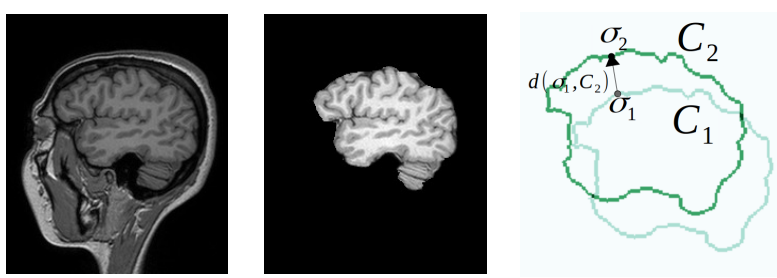

(a) MR image (b) Brain extraction (c) Hausdorff distance

Figure 4.3: Example of brain extraction

4.1.3 Brain Segmentation

Brain segmentation is the task of partitioning the brain image (MRI in our case), into the following segments: background, white matter, gray matter and CSF. This process is of a great importance for brain MR image analysis, especially for therapy planning and also for clinical research. Sampling artifacts, results in poor signal to noise and blurry edges, and also loss of anatomical fine details, will probably leads to bad segmentation performance. We suggest a way to evaluate and compare different MRI reconstruction methods based on segmentation results. We create a reference segmentation by extracting the brain (using BET [**?**]) from the original fully-sampled image and run a brain segmentation algorithm (FAST [**?**]). Then, we did the same process for all the reconstruction methods and compared the segmentation results to the reference.

The measure used for segmentations comparison is the Dice score [**?**] between the original and the reconstructed image segments. Dice score is a measure of sets similarity which gets the values between 0 (no similarity) to 1.0 (max similarity). Denotes by $S_{i,j}$ the set of pixels in segment j for reconstruction method i, the Dice score between this method to the reference is:

$$DICE(S_{ref,j}, S_{i,j}) = \frac{2 \cdot |S_{ref,j} \cap S_{i,j}|}{|S_{ref,j}| + |S_{i,j}|} \tag{4.2}$$

Dice values for different sampling ratios are presented in Table 4.5. Our methods achieved the best Dice scores for all brain tissues.

DICE	Factor 2.5			Factor 4			Factor 6		
Method	White	Gray	CSF	White	Gray	CSF	White	Gray	CSF
Zero-filled	0.882±0.08	0.826±0.05	0.796±0.05	0.718±0.10	0.644±0.05	0.627±0.05	0.599±0.12	0.466±0.07	0.050±0.06
CS-MRI	0.942±0.05	0.910±0.03	0.868±0.03	0.871±0.10	0.805±0.08	0.770±0.05	0.708±0.14	0.639±0.08	0.621±0.07
IM-CNN-L2	0.947±0.02	0.917±0.02	0.887±0.02	0.903±0.03	0.853±0.02	0.828±0.02	0.741±0.14	0.681±0.08	0.674±0.07
CNN-L2	0.948±0.02	0.919±0.02	0.891±0.02	0.888±0.06	0.836±0.04	0.813±0.03	0.836±0.09	0.770±0.06	0.747±0.06
Proposed	**0.954±0.01**	**0.928±0.02**	**0.900±0.002**	**0.903±0.06**	**0.858±0.04**	**0.833±0.03**	**0.851±0.09**	**0.789±0.06**	**0.767±0.06**

Table 4.5: Segmentation Dice score for different sampling ratios

Visual comparison for sampling factor 6 is shown in Figure 4.4. The first and the second rows are the reconstructed images with zoom in of red ROI. The third row is the extracted brain and the last row is the calculated segmentation. Each column represents different reconstruction method. MRIs reconstructed by using the suggested adversarial method have stronger contrast and no significant aliasing or artifacts. In addition the brain extraction and the segmentation are more accurate. Additional examples for factor 4 and 2.5 can be found in Figures 4.5, 4.6.

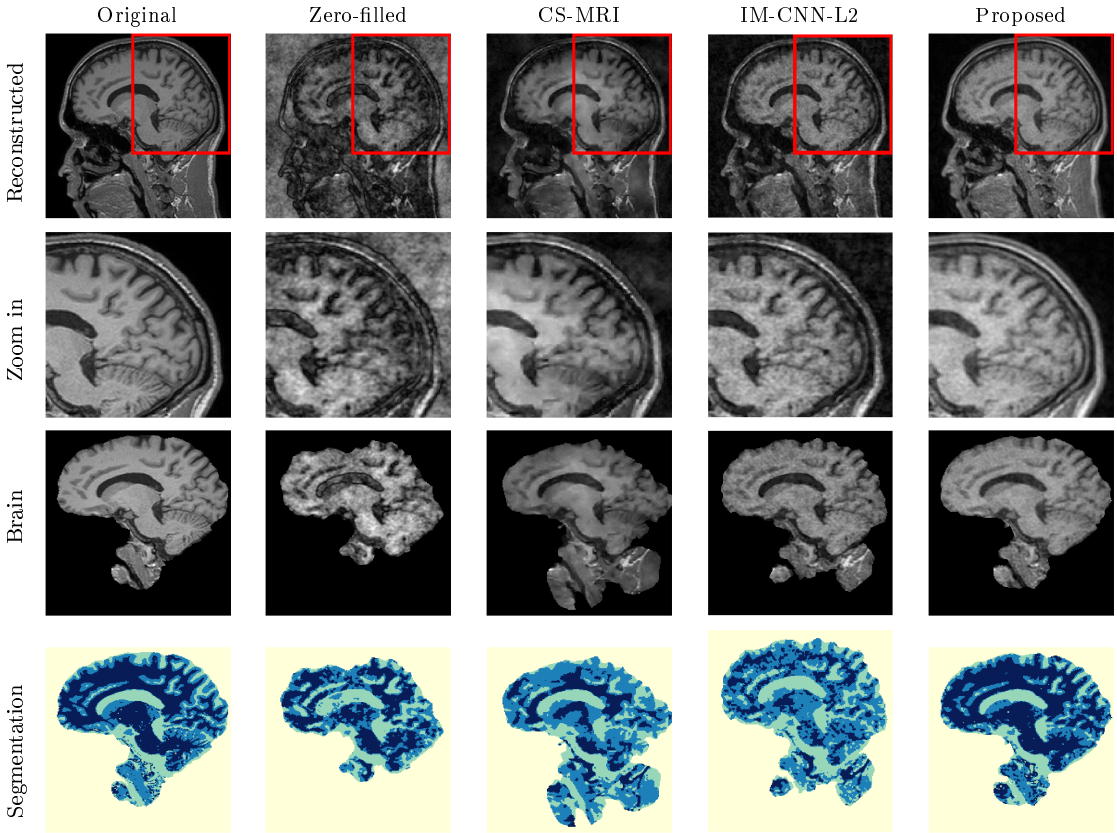

Figure 4.4: Examples of reconstructed MR images from under-sampled k-space - Factor 6.

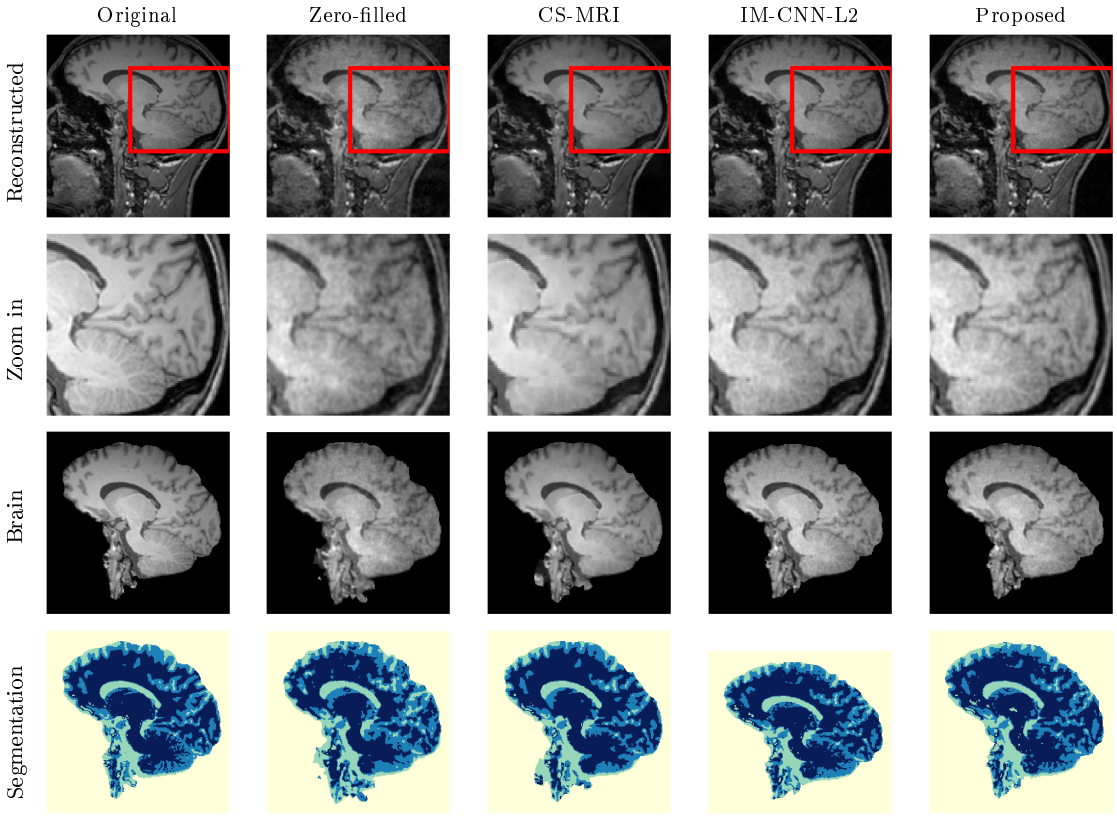

Figure 4.5: Examples of reconstructed MR images from under-sampled k-space - Factor 4.

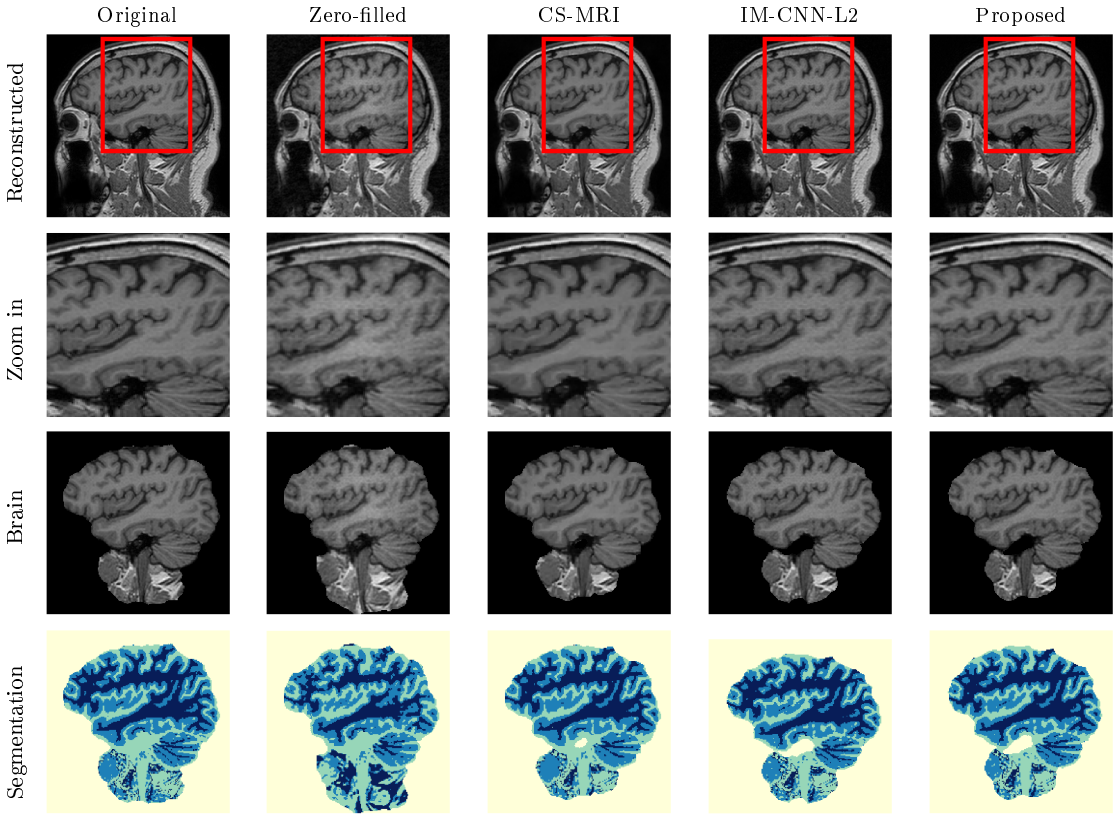

Figure 4.6: Examples of reconstructed MR images from under-sampled k-space - Factor 2.5.

4.2 Phase Encoding Sampling

The training data consists of 55 $3D$ brain MRI (T1) scans of different patients, acquired by 1.5T MR machine with resolution of 256×256 pixels. We used $3k$ 2D slices for training and $1.2k$ for testing. In order to create k-space images for training, inverse orthonormal 2D FFT is applied to the fully-sampled MR images. We sample the k-space images along the phase axis using Cartesian binary mask, while keeping 5% from the centered phases, which is the area that contains 95% of the energy. Data augmentation is created by random offsets of the proposed mask and image flipping. This leads us to reconstruction of the MR image from only 52% of the original k-space data.

The generator is composed of 5 blocks of CONV-BatchNorm-ReLU, with output channels $16, 32, 64, 32, 8$, respectively. The last layer is CONV with two outputs channels (for real and imaginary parts). The discriminator is composed of 4 blocks of CONV-Pool-BatchNorm-LReLU with output channels $8, 16, 32, 16$ and one fully-connected layer. All CONV layers kernel size is 3×3. All weights

was initialized by Xavier [?]. We used Adam solver with fixed learning rate of 0.0005 and set k_g to 20.

We compare the proposed method to reconstruction results obtained by using a conventional compressed sensing method CS-MRI [?] and Zero-filling. In addition, we trained a generator (G) using only L2 loss (CNN-L2). The same sampling mask was used for all cases. Visual comparison is shown in Figure 4.7. MRIs reconstructed by using the suggested adversarial loss have stronger contrast and no significant aliasing or artifacts. Quantitative evaluation using PSNR values is presented in Table 4.6. Note that the proposed method outperforms the other methods.

PSNR	Mean	std
Zero-filled	30.48	0.13
CS-MRI	36.78	0.4
CNN-L2	37.12	0.82
Proposed	**37.95**	0.6

Table 4.6: Error in PSNR

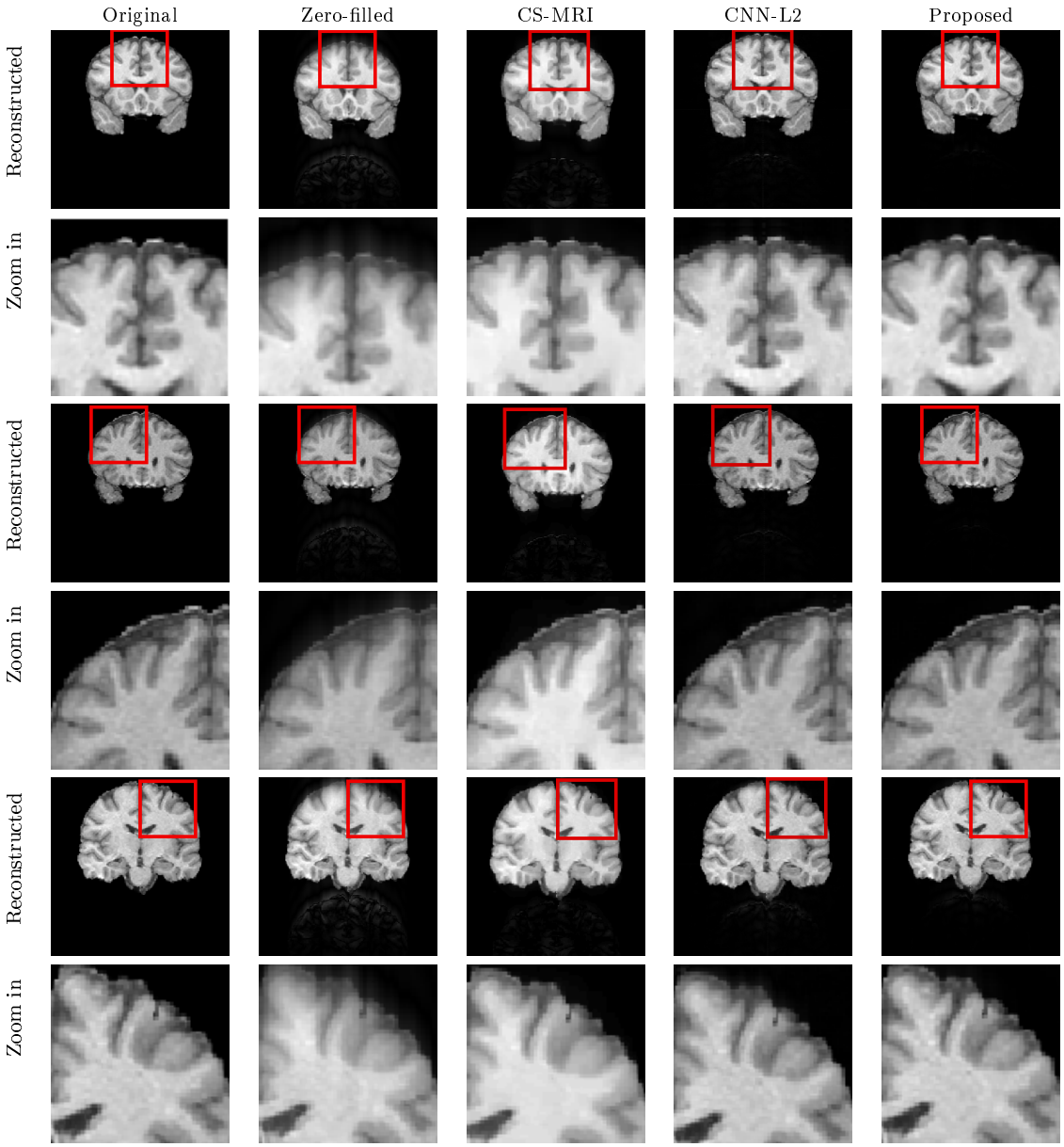

Figure 4.7: Examples of reconstructed MR images from under-sampled k-space.

Chapter 5

Summary and Discussion

5.1 Discussion

We proposed a practical, software-only framework, based on deep learning, for accelerating MRI acquisition, while maintaining anatomically meaningful imaging. This is accomplished by partial MRI sampling, while using an adversarial neural network to directly estimate the missing k-space samples (based on the real k-space distribution). Promising image reconstruction results are obtained for 3T and 1.5T brain MRI, from large publicly available dataset, where only 40%, 25% and 16.6% of the raw samples of each scan are used.

Our method produce more clinically acceptable reconstructions compared with the methods being tested in the terms of PSNR and SSIM. We also perform tissue segmentations and measure the performance using the Dice scores, with respect to those obtained by using the original fully-sampled images. Better Dice score for white matter, gray matter, and CSF were achieved for all sampling factors. Moreover, lower Hausdorff distances indicates the quality of the proposed method in terms of general brain shape. Comparing to CS, our reconstruction method preserve the brain shape better, as seen in Figures 4.4, 4.5, 4.6.

Additional advantage of the proposed method is the runtime. A few days are required for training the generator. Once the network is optimized, the reconstruction for a single test image is done in less than 10 msec, almost two orders of magnitude faster than the widely used CS. This fact makes it possible to use it in a real time manner. Future work will concentrate on generation of MRI in the presence of pathologies.

5.1.1 Acknowledgment

This research is partially supported by the Israel Science Foundation (T.R.R. 1638/16) and the IDF Medical Corps (T.R.R.)

Bibliography

תקציר

אחד האתגרים הגדולים בתחום של דימות תהודה מגנטי (MRI) הוא האצת הרכישה לצרכים קליניים. מעבר לשיפור בנוחות המטופלים והוזלת עלויות, סריקות מהירות יותר הכרחיות לבדיקות אשר רגישות לשינויים בזמן, כמו למשל סריקות לב, ריאות ועוברים. סריקות אלו רגישות לתנועות של המטופל ובכך איכות הסריקה נפגעת.

יתר על כך, רכישה מהירה יתר תשפר רזולוציה זמנית בסריקות דינמיות, כמו fMRI ו-DC-MRI. השיטות הקיימות כיום אכן מקצרות את זמן הסריקה באיכות יחסית טובה, אך לעיתים אורכות זמן רב ואפילו מייקרות את החומרה הנדרשת לסריקה.

אנחנו מציגים פתרון פרקטי תוכנתי בלבד, המבוסס על למידה עמוקה להאצת רכישת ה- MRI של המוח, וזאת תוך כדי שימור המבנה האנטומי. פתרון זה מושג על ידי דגימה חלקית של המידע הגולמי ב-MRI הנקרא גם k-space, ושחזור בעזרת רשת נוירונים אדברסית המשערכת את הדגימות החסרות. הרשת בנויה על משחק סכום אפס בין שתי רשתות שונות. האחת משערכת דגימות חסרות והשנייה מייצרת מעין פידבק-משוב על תוצאת הראשונה. יחד עם שילוב אילוצי נורמת L2, השיטה שלנו מייצרת שחזורים באיכות טובה, על מאגר מידע גדול, עבור מספר מקדמי האצה, 2.5, 4 ו-6.

על מנת לוודא שאכן התמונות המשוחזרות שומרות על המבנה האנטומי, ועל השימוש הקליני שלהן, בצענו מספר ניסויים אשר יכולים להעיד על כך. השוונו תוצרי סגמנטציה בין התמונות המשוחזרות לבין התמונה המלאה בעזרת מדד ה Dice ומדד Hausdorff distance, ואלו המחישו את איכות השחזור באמצעות השיטה המוצעת, בהשוואה לשאר השיטות המוצגות בעבודה זו.

אוניברסיטת בן גוריון בנגב

הפקולטה למדעי ההנדסה

המחלקה להנדסת חשמל ומחשבים

האצת דימות תהודה מגנטית באמצעות רשתות נוירונים אדברסריות

חיבור זה מהווה חלק מהדרישות לקבלת התואר "מוסמך למדעי ההנדסה" (M.Sc.)

מאת: אוהד שטרית

בהנחיית: ד"ר תמי ריקלין-רביב

חתימת הסטודנט: _____ תאריך 28/02/2018

חתימת המנחה: _____ תאריך_____

חתימת יו"ר הועדה המחלקתית: _____ תאריך_____

תשע"ח פבואר 28

אוניברסיטת בן גוריון בנגב
הפקולטה למדעי ההנדסה
המחלקה להנדסת חשמל ומחשבים

האצת דימות תהודה מגנטית באמצעות רשתות נוירונים אדברסריות

חיבור זה מהווה חלק מהדרישות לקבלת התואר "מוסמך למדעי ההנדסה" (M.Sc.)

מאת: אוהד שטרית

בהנחיית: ד"ר תמי ריקלין-רביב

תשע"ח פבואר 28